AIP Journal of Applied Physics

Network structure and thermal stability study of high temperature seal glass

K. Lu and M. K. Mahapatra

Citation: Journal of Applied Physics **104**, 074910 (2008); doi: 10.1063/1.2979323
View online: http://dx.doi.org/10.1063/1.2979323
View Table of Contents: http://scitation.aip.org/content/aip/journal/jap/104/7?ver=pdfcov
Published by the AIP Publishing

Network structure and thermal stability study of high temperature seal glass

K. Lu[a] and M. K. Mahapatra[b]
Department of Materials Science and Engineering, Virginia Polytechnic Institute and State University, Blacksburg, Virginia 24061, USA

(Received 10 June 2008; accepted 14 July 2008; published online 6 October 2008)

High temperature seal glass has stringent requirement on glass thermal stability, which is dictated by glass network structures. In this study, a $SrO-La_2O_3-Al_2O_3-B_2O_3-SiO_2$ based glass system was studied using nuclear magnetic resonance, Raman spectroscopy, and x-ray diffraction for solid oxide cell application purpose. Glass structural unit neighboring environment and local ordering were evaluated. Glass network connectivity as well as silicon and boron glass former coordination were calculated for different $B_2O_3:SiO_2$ ratios. Thermal stability of the borosilicate glasses was studied after thermal treatment at 850 °C. The study shows that high B_2O_3 content induces BO_4 and SiO_4 structural unit ordering, increases glass localized inhomogeneity, decreases glass network connectivity, and causes devitrification. Glass modifiers interact with either silicon- or boron-containing structural units and form different devitrified phases at different $B_2O_3:SiO_2$ ratios. B_2O_3-free glass shows the best thermal stability among the studied compositions, remaining stable after thermal treatment for 200 h at 850 °C. © *2008 American Institute of Physics*. [DOI: 10.1063/1.2979323]

I. INTRODUCTION

Glass is the most preferred candidate as planar solid oxide fuel and electrolyzer cell seals.[1] To be used as a seal, one of the most important and challenging criteria is thermal stability at solid oxide cell operating temperature for a long time (>50 000 h). A new glass based on $SrO-La_2O_3-Al_2O_3-B_2O_3-SiO_2$ (SABS) system has been reported to demonstrate excellent thermal properties.[2] However, La_2O_3 and B_2O_3 degrade the thermophysical stability of the SABS glass system and contribute to devitrification by forming $LaBO_3$.[3,4] Also, B_2O_3 may evaporate in the form of volatile HBO_2 and $B(OH)_3$ species in the presence of water steam at cell operating temperatures.[5,6] There is a need to understand the SABS glass network structure in order to improve the thermal stability of the glass system.

The key aspects regarding glass structure are network connectivity and homogeneity, which directly affect the thermal stability of a glass. Connectivity in a glass structure is described by the number and arrangement of bridging and nonbridging oxygen atoms, which link the structural units to their neighbors. Glass homogeneity is directly related to the distribution of different structural units and modifiers. If there is heterogeneity, such as structural unit ordering or distribution preference in a glass, even if in small localized regions, glass can devitrify easily.[7]

Nuclear magnetic resonance (NMR) spectroscopy has been used to analyze glass structure differences. The temporal evolution of the coordination environments of boron atoms in borosilicate glasses was studied. The temperature dependence of boron speciation was found to be the most important source for the production of configurational entropy in these glasses, signifying a direct link between structure, configurational entropy, and viscous flow.[8] The structure of $BeO-SiO_2$ glasses with up to 20 mol % BeO was studied with ^9Be and ^{29}Si NMR spectroscopic techniques. The NMR results showed nanoclusters of corner-shared BeO_4 and highly strained corner-shared SiO_4 network.[9] Distributions of aluminum among the structural units in $CaO-Al_2O_3-SiO_2$ and $MgO-Al_2O_3-SiO_2$ glasses were investigated by ^{29}Si and ^{27}Al magic angle spinning (MAS) NMR. Taking the convention that the silicate units with four bridging oxygen atoms, three bridging oxygen atoms, two bridging oxygen atoms, one bridging oxygen atom, and zero bridging oxygen atom are denoted as Q^4, Q^3, Q^2, Q^1, and Q^0, respectively. The results indicated that aluminum is largely in Q^4 sites, except in Al-rich glasses where it is also in Q^3 sites.[10] ^{17}O enriched calcium and potassium aluminoborosilicate glasses were studied by ^{11}B, ^{27}Al, and ^{17}O NMR.[11] Dramatic differences in boron and oxygen speciation demonstrate a large effect of the modifier cations on glass former mixing behavior and stabilization of nonbridging oxygen atoms.

Raman spectroscopy is another important technique that can identify the structural units present in a glass.[12–14] For chalcogenide glasses, Raman scattering played a pivotal role in elucidating the molecular structures and identifying domains of intermediate phases.[15] Raman spectra from $Na_2O-CaO-MgO-Al_2O_3-SiO_2$ system were interpreted in terms of structural alteration as the composition was altered from the binary end members to more complicated glasses.[16] Addition of CaO and MgO to Na_2O-SiO_2 glasses acted only to increase the disorder of the network slightly. Addition of Al_2O_3 greatly modified the network. In the $Na_2O \cdot R_2O_3 \cdot SiO_2$ ($R=Al,B$) system, Raman spectroscopy showed that B_2O_3

[a]Author to whom correspondence should be addressed. Electronic address: klu@vt.edu. Tel.: +1 540 231 3225. FAX: +1 540 231 8919.
[b]Electronic mail: mkmanoj@vt.edu.

induces destruction of the Q^3 species and the creation of highly charged Q^2 and Q^1 species, as well as fully connected Q^4 silicate units.[17]

The current study is focused on understanding the network structure and thermal stability of the SABS glass system. To examine the SABS glass structural evolution with B_2O_3:SiO_2 ratio change, MAS NMR, and Raman spectroscopy studies have been carried out. Structural evolution data obtained from NMR and Raman spectroscopy, two complementary methods for giving detailed information about borosilicate glass structure, provide the best knowledge about the devitrification resistance of the studied SABS glass system. NMR gives access to the BO_3/BO_4 ratio and to the identification of the different structural unit environment, whereas Raman spectroscopy gives information on glass structural unit types, ordering, and distribution. Glass network connectivity and coordination have been calculated for different SABS glasses. To examine the SABS glass thermal stability at high temperatures, x-ray diffraction (XRD) study has been carried out for the SABS glasses thermally treated at 850 °C. The evolution of devitrified phases versus the SABS glass compositions is discussed. The correlation between the glass network structure and thermal stability is established.

II. EXPERIMENTAL PROCEDURE

A. Glass preparation

SABS glass samples were prepared with conventional quenching method. $SrCO_3$ (99.9%, Sigma Aldrich, St. Louis, MO), La_2O_3 (99.98%), Al_2O_3 (99.95%), B_2O_3 (99.98%), and SiO_2 (99.8%) (all oxides from Alfa Aesar, Ward Hill, MA) at designed ratios were mixed in a ball mill for overnight. The mixed powders were heated in a platinum crucible in a box furnace (Lindberg, Model 51314, Watertown, WI) to 1100 °C and kept there for 1 h for $SrCO_3$ to decompose. After that, the mixture was heated to 1400 °C for 4 h. The heating rate was 10 °C min^{-1}. The molten glass was quenched into a graphite mold.

All the glass compositions had 40 mol % of SrO, La_2O_3, and Al_2O_3 at fixed SrO:La_2O_3:Al_2O_3 ratios. The total amount of B_2O_3 and SiO_2 was 60 mol % and the Al_2O_3 content was 5.0 mol %. B_2O_3:SiO_2 ratio was varied from 0 to 1.4. The compositions were abbreviated as SABS-0, SABS-5, SABS-10, SABS-15, and SABS-35 in this study. The numbers represent the mole percent of B_2O_3 in each composition. The formation of SABS glasses after quenching was confirmed by XRD study.

B. NMR experiment

The ^{11}B, ^{29}Si, and ^{27}Al MAS NMR spectra of the SABS glass samples were collected with Bruker MAS probes and a Bruker Avance 500 spectrometer equipped with a widebore ultrashield magnet operating at a Larmor frequency of 160.4, 99.5, and 130.3 MHz for ^{11}B, ^{29}Si, and ^{27}Al, respectively. The applied magnetic field was 11.7 T. ^{11}B and ^{27}Al MAS NMR spectra were collected with a 4 mm probe. Crushed SABS glass samples were spun in Si_3N_4 and ZrO_2 rotors at 15 kHz. All ^{11}B and ^{27}Al MAS spectra were collected using nonselective rf pulses with 15° tip angle and a recycle delay of 2 s. Approximately 500 to 1000 free induction decays were averaged to obtain each spectrum. The ^{11}B and ^{27}Al chemical shifts were externally referenced to 0.1*M* $Na_2B_4O_7$ solution at 9.8 ppm and to 1*M* $AlCl_3$ solution at 0 ppm, respectively. For ^{29}Si MAS NMR experiments, the crushed glass samples were spun in a ZrO_2 rotor with a 7 mm Bruker MAS probe. The spectra were collected using rf pulses with 60° tip angle and a recycle delay of 30 s. Approximately 4000 free induction decays were averaged to obtain each spectrum. ^{29}Si chemical shifts were externally referenced to tetramethyl silane at 0 ppm.

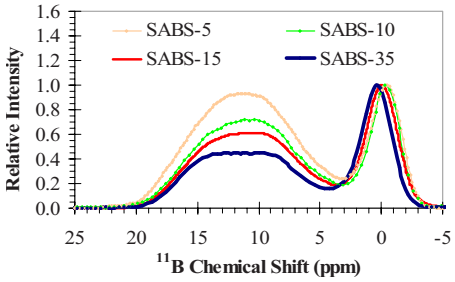

FIG. 1. (Color online) ^{11}B MAS NMR spectra of SABS glasses.

C. Raman spectroscopy

For Raman spectroscopy analysis of the SABS glass compositions, quenched glass samples were polished to optical finish. Raman spectra of the polished samples were collected in 200–1600 cm^{-1} wave number range using a Raman spectrometer (JY Horbia LabRam HR 800, Horiba Ltd., Japan) with a charged coupled device detector and Labspec software. The light source was a 514.57 nm argon laser at 50 mW power and 400 s exposure time. The spectra were later corrected to remove background noise and temperature effects.[18] For data analysis, the Raman spectra were fitted to Gaussian bands without any restriction to deconvolute the superimposed Raman peaks.[19,20] The curve fitting was done with a GRAMS/AI (7.02) software (Themo Fisher Scientific, Inc. Waltham, MA).

D. Phase analysis

For thermal stability study, the SABS glass samples were put on a platinum foil and heated to 850 °C at the same heating and cooling rate of 5 °C min^{-1}. The samples were thermally treated at 850 °C for 50–200 h. XRD studies were carried out in an X'Pert PRO diffractometer (PANalytical B.V., EA Almelo, The Netherlands) to identify the devitrified phases in the thermally treated samples. The scan rate was 0.0020° s^{-1} with Cu K_α radiation ($\lambda = 1.5406$ Å) and a nickel filter.

III. RESULTS AND DISCUSSIONS

A. Glass structural unit environment

The ^{11}B MAS NMR spectra of the SABS glasses are shown in Fig. 1. SABS-0 composition is not included since it is B_2O_3 free. The broad powder pattern on the left (12 ppm peak) and the narrow Gaussian curve on the right (0 ppm peak) can be readily assigned to BO_3 (trigonal boron species)

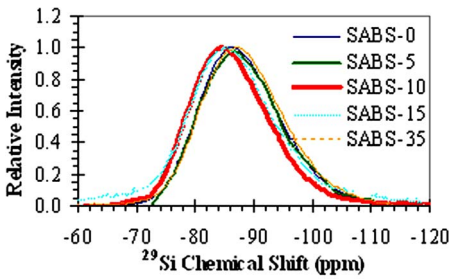

FIG. 2. (Color online) ^{29}Si MAS NMR spectra of SABS glasses.

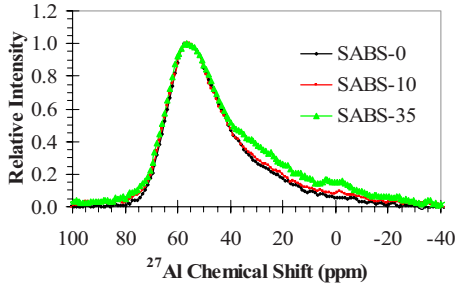

FIG. 3. (Color online) Al ^{27}MAS NMR spectra of SABS-0, SABS-10, and SABS-35 glasses.

and BO_4 (tetrahedral boron species), respectively. Direct simulation of these spectra is difficult due to the heterogeneous broadening of the BO_3 line shape. Instead, these spectra are all normalized to the highest intensity of the BO_4 line shape. The relative intensity of the BO_3 peak maximum is used as a relative measure of BO_3:BO_4 ratio. As seen from Fig. 1, the BO_3:BO_4 ratio in the SABS glasses decreases significantly and systematically with B_2O_3 content increase. This means higher B_2O_3 content induces BO_4 glass structural unit formation. The fundamental cause is that the bonding between BO_3 and SiO_4 (trigonal and tetrahedral network units) is unfavorable because of their relatively high local charge concentrations. The degree of coordination with SiO_4 for BO_3 is less than that for BO_4, even though SiO_4 and BO_4 coordination needs to be further examined.[21]

Previous ^{11}B NMR studies of borosilicate glasses have shown that BO_3:BO_4 ratio is independent of B_2O_3:SiO_2 ratio at low modifier contents.[22] However, at high modifier concentrations that are characteristic of the SABS glasses studied here, the BO_3:BO_4 ratio is expected to decrease at a rapid rate with B_2O_3 content increase.[22] This structural scenario is consistent with the compositional evolution of the ^{11}B MAS NMR spectra shown in Fig. 1. As it indicates, the BO_3:BO_4 ratio progressively decreases from SABS-5 to SABS-35. It is also interesting to note that the ^{11}B chemical shift for the BO_3 site is located around 11 ppm, indicating that these sites contain at least one nonbridging oxygen atom forming a T^2 boron site (where T stands for "ternary" by analogy to the Q^n nomenclature for quaternary silicon).[23] In addition, the ^{11}B chemical shift for the BO_4 sites shows systematic increase from −0.50 to 0.44 ppm with increasing B_2O_3 content from SABS-5 to SABS-35. This result means that increasing ^{11}B chemical shift for the BO_4 sites causes less sharing of oxygen between BO_4 and SiO_4 tetrahedra from SABS-5 to SABS-35.[24] The bonding between BO_4 and SiO_4 is better than that between BO_3 and SiO_4 but keeps decreasing from SABS-5 to SABS-35.

The ^{29}Si MAS spectra of the SABS glasses are shown in Fig. 2. These spectra show a slightly asymmetric peak that centers from −85 to −87 ppm. The absence of B_2O_3 in the SABS-0 glass and the small amount of Al_2O_3 (in comparison to SiO_2) make the ^{29}Si peak assignment straightforward. The main structural unit is Q^3 (chemical shift of ~−87 ppm).[25] The shoulder near −100 ppm indicates the presence of a small amount of Q^4 species with one or two aluminum as next-nearest neighbors. The ^{29}Si MAS NMR spectra of SABS-5 to SABS-10 are very similar to that of SABS-0, in spite of the increase in the B_2O_3 content. This observation implies that SiO_4 tetrahedrals in these glasses share oxygen with BO_3 units to a certain extent. However, as mentioned above, the systematic change in the ^{11}B chemical shift of BO_4 units in these glasses indicates preferred linking of BO_4 and SiO_4 tetrahedra, which begins to influence the ^{29}Si chemical shift in SABS-15 and SABS-35 glasses. In SABS-35, characterized by the highest B_2O_3 content and the lowest BO_3:BO_4 ratio, the entire ^{29}Si MAS NMR spectrum shifts to higher chemical shift values indicating either the formation of Q^2 species or Q^3 species linked with multiple B^{IV} next-nearest neighbors. SABS-15 glass reveals a chemical shift in between those of SABS-10 and SABS-35. This means at low B_2O_3 content SiO_4 structural units may bond with BO_3 structural units. As B_2O_3 content increases, BO_4 content increases; SiO_4 structural units are more likely to bond with BO_4 structural units.

For clarity, only the ^{27}Al MAS NMR spectra of SABS-0, SABS-10, and SABS-35 glasses are shown in Fig. 3. These spectra are nearly identical and dominated by a strong, asymmetric peak positioned at 56 ppm that corresponds to tetrahedrally coordinated aluminum with a distribution of quadrupolar coupling coefficients, typical of oxide glasses. This means Al_2O_3 mainly acts as a glass former in the SABS glasses. As reported before, the addition of Al_2O_3 can reduce the degree of phase separation in the SABS glasses; possibly by the formation of B–O–Al–O–Si linkages.[4] These two observations are consistent. The ^{27}Al MAS NMR spectrum of SABS-35 displays clear but small shoulders near 28 and 0 ppm that correspond to small concentrations (a few %) of five- and six-coordinated aluminum.[11] This result is not surprising, as the structure of this glass with its low SiO_2 content would have a strong presence of boroaluminate network. Such networks are typically characterized by the presence of five- and six-coordinated aluminum atoms forming Al–O–B linkages.[11] This observation indicates that whether aluminum acts as a glass former or as a glass modifier depends on the B_2O_3 content in borosilicate glass. Even though Al_2O_3 mostly acts as a glass former, B_2O_3 content increase could change it to a glass modifier. The quantity of Al_2O_3 as a glass former in the SABS glasses requires ^{27}Al triple-quantum MAS NMR studies.

B. Glass structural unit local ordering

To understand the atomic level bonding structure of the SABS glasses, deconvoluted Raman spectra for the SABS

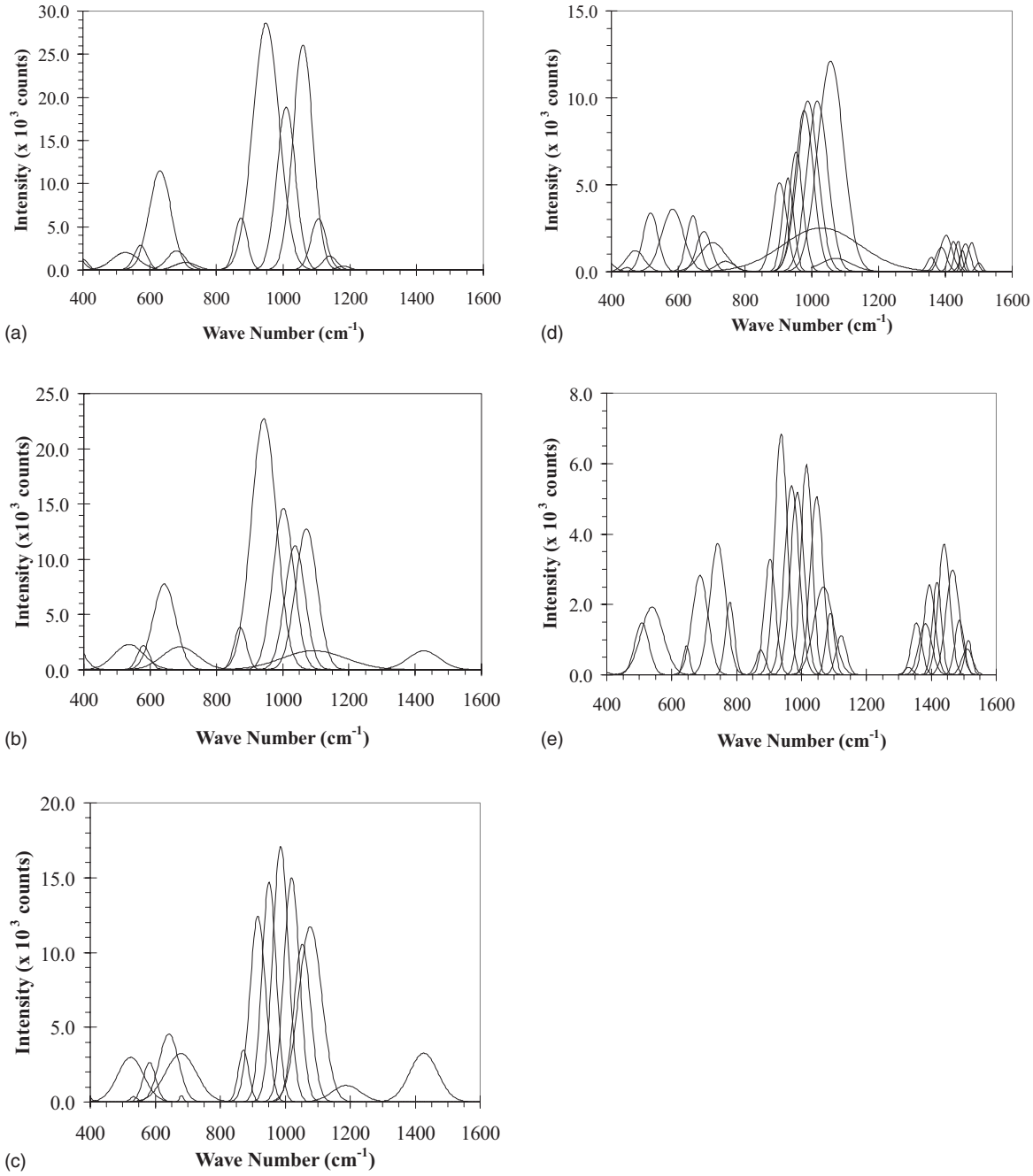

FIG. 4. Deconvoluted Raman peaks for (a) SABS-0, (b) SABS-5, (c) SABS-10, (d) SABS-15, and (e) SABS-35.

glasses are shown in Fig. 4. Before analyzing the structural units and coordination of the SABS glasses, it is beneficial to examine silicate glass and borate glass structures first. In silicate glass, there are four major Raman peaks representing the nature and contribution of the different silicate structural units. The 1050–1100 cm^{-1} wave number region describes the stretching motion of the Q^3 units. The 950–1000 cm^{-1} wave number peak describes the stretching motion of the Q^2 units. The 900 cm^{-1} wave number peak reflects the pyrosilicate composition with the Q^1 units. The 850 cm^{-1} wave number peak represents the Q^0 units.[13] The 400–700 cm^{-1} wave number peak represents the delocalized vibration of Si–O–Si from mixed stretching and bending modes.[17] In borate glass, the 1200–1600 cm^{-1} peak describes the B-O^- (O^- denotes the nonbridging oxygen) stretching mode within the chain and ring metaborates.[26] The low frequency region of the 1400 cm^{-1} band can be attributed to BO_3 trigonals linked to BO_4 tetrahedrals, exhibiting a lower vibration frequency as a result of π^- electronic interaction.[27] Based on the above understanding, peaks in different wave number ranges of the SABS glass spectra can be identified.

For the SABS-0 glass, no peaks are detected in the 1300–1600 cm^{-1} range, corresponding to the Raman peaks from B_2O_3. This is easy to understand because the SABS-0 glass is B_2O_3-free. For the SABS-5 and SABS-10 glasses, the 1426 cm^{-1} peak can be assigned to localized stretching vibration of B–O^- bonds from metaborate units.[16] For the SABS-15 glass, the presence of 1357 and 1387 cm^{-1} peaks indicate the B–O^- vibrations in a large borate network.[17] The peaks at 1424, 1452, 1460, and 1501 cm^{-1} can be as-

signed to metaborate units and localized stretching vibration modes of $B-O^-$ bonds, as for the 1426 cm^{-1} wave number peak in the SABS-5 and SABS-10 glasses.[16] In addition, the 1479 cm^{-1} peak is attributed to the stretching mode of disordered BO_3 triangles.[10] The 1402 and 1438 cm^{-1} peaks cannot be identified. In the SABS-35 glass, the 1487 cm^{-1} peak can be attributed to the stretching mode of disordered BO_3 triangles.[10] With the increasing intertetrahedral angle, one peak for the borate glass splits into three peaks, one at lower wave number, another at higher wave number, and one remaining at the same wave number.[28] For the SABS-35 glass, the peaks at 1354, 1382, and 1394 cm^{-1} can be assigned to the splitted 1380 cm^{-1} peak identified for the $B-O^-$ vibration.[17] The peaks at 1466, 1510, and 1514 cm^{-1} can be assigned to localized stretching vibration of $B-O^-$ bonds.[16] The 1330, 1417, and 1443 cm^{-1} peaks cannot be identified. In general, Raman peak splitting in this high wave number region increases with B_2O_3 content increase. From this analysis, it can be concluded that B_2O_3 progressively affects the glass network structure by $B-O^-$ vibration and stretching modes; high amount of B_2O_3 also causes more borate structural unit ordering.[17]

In the 800–1200 cm^{-1} region, for the SABS-0 glass, the weak 1143 and 1180 cm^{-1} peaks correspond to the splitted 1060–1200 cm^{-1} peak in vitreous silica.[29] These peaks describe the Q^4 units. The 1060 and 1105 cm^{-1} peaks are from the Q^3 units. The 949 and 1010 cm^{-1} peaks are from the Q^2 units. The 872 cm^{-1} peak is from the Q^0 units. For the SABS-5 glass, no Q^4 structural units are detected. The 1036, 1072, and 1094 cm^{-1} peaks are from the Q^3 units. The 943 and 1003 cm^{-1} peaks are from the Q^2 units. The 872 cm^{-1} peak is from the Q^0 units. In the SABS-10 glass, the weak peak at 1188 cm^{-1} is from the diborate groups. The peaks at 1053 and 1077 cm^{-1} are from the Q^3 units. The peaks at 951, 986, and 1020 cm^{-1} are from the Q^2 units. The peak at 916 cm^{-1} is from the Q^1 units. The 872 cm^{-1} peak is from the Q^0 units. This means the glass structure continues to become less connected, and borate structural units start to play a role in the glass network. For the SABS-15 glass, the 1056 cm^{-1} peak is from the Q^3 units. The 952 to 1028 cm^{-1} peaks are from the Q^2 units. The 929 cm^{-1} peak can be attributed to $Si(OAl)_3$ units with one bridging oxygen atom.[30] The 904 cm^{-1} peak is also from the Q^1 units. For the SABS-35 glass, the 1122 cm^{-1} peak is attributed to the diborate groups. The 1068 and 1089 cm^{-1} peaks are attributed to the Q^3 units. The 970–1047 cm^{-1} peaks are attributed to the Q^2 units. The 937 cm^{-1} peak is from orthoborate units. The 903 cm^{-1} peak corresponds to the Q^1 units. The 875 cm^{-1} peak is from the Q^0 units. Some BO_4 structural units appear to be isolated, a continuing trend of more B_2O_3 involvement in the SABS glass network. Overall, this 800–1200 cm^{-1} range peak splitting evolution shows that as B_2O_3 content increases, there are increased weakening of the SABS glass network and local ordering of the silicate and borate structural units.

In the 400–800 cm^{-1} region, for the SABS-0 glass, the 619 and 641 cm^{-1} peaks are from the Q^2 units. The 605 cm^{-1} peak is from the Q^3 units. For the SABS-5 glass, the 690 cm^{-1} peak is from the Q^1 units. The 643 cm^{-1} peak is from the Q^2 units. The 537 and 580 cm^{-1} peaks are from the BO_4^- units in anionic rings. Borate structural units appear when the glass composition changes from SABS-0 to SABS-5. For the SABS-10 glass, the 679 and 680 cm^{-1} peaks are from the Q^1 units. Some metaborate units may also contribute to these peaks. The 642 cm^{-1} peak is from the Q^2 units. The peaks at 524, 534, and 582 cm^{-1} are from BO_4^- anionic rings. For the SABS-15 glass, the 471 cm^{-1} peak is from the Q^3 units but may also have contribution from the bending mode of B–O–B, B–O–Si, and Si–O–Si linkages.[22] The 446 cm^{-1} peak is from the Q^4 units. The 517 and 583 cm^{-1} peaks are from BO_4^- units. The 741–744 cm^{-1} peaks are attributed to BO_4^- tetrahedral units with nonbridging oxygen atoms. The 677 and 704 cm^{-1} peaks are attributed to the Q^1 units along with some metaborate units. The 644 cm^{-1} peak is attributed to the Q^2 units. In the SABS-35 glass, simultaneous appearance of 508, 645, 779, and 937 cm^{-1} peaks confirms the presence of pentaborate structural units. The 742 cm^{-1} peak is attributed to BO_4^- tetrahedrals. The 467 cm^{-1} peak is from the B–O–Si linkages. The 688 cm^{-1} peak is attributed to B–O–Si linkages from the Q^1 units. The 539 cm^{-1} peak is attributed to the BO_4^- units. As it shows, from SABS-0 to SABS-35, T^n peak splitting increases. This means the SABS glass structure is increasingly affected by B_2O_3, structural units become more localized, and mixed bonding also increases.

C. Connectivity

Thermal properties of a glass depend on the presence of atomic level structural units, their relative arrangement, and the amounts of bridging and nonbridging oxygen atoms.[31] This is because these structural parameters determine the glass network connectivity. If a glass has high connectivity, then it is likely to be stable and resistant to devitrification. If a glass has low connectivity, then it is likely to devitrify. Increasing nonbridging oxygen content decreases glass connectivity. In the SABS glass system, B_2O_3 becomes more dominant in the glass structure as its content increases. Along with the increase in the relative percent of BO_4 structural units, the absolute content of BO_3 structural units still increases. This leads to more chain and ring metaborate and even orthoborate (for SABS-35) contents and increasingly broken SiO_4 tetrahedral network. As a result, connectivity decreases.

Quantitatively, glass network connectivity ψ can be defined as follows based on prior knowledge of degree of network formation:[32]

$$\Psi = \frac{\left[\frac{\sum Z_i(F_iV_i)}{\sum Z_iV_i}\right]_{\text{Network Former}}}{\left[\frac{\sum F_iV_i}{\sum V_i}\right]_{\text{Network Former+Modifier}}} \times \frac{\sum O^+}{\sum O^- + \sum O^+}, \quad (1)$$

where F_i is the field strength of oxide i in a glass system, V_i is the amount of oxide i in vol %, and Z_i is the atomic number of oxide i. The first term in Eq. (1) considers the bonding effect of cations that are present in a glass network. The

TABLE I. Calculated glass network connectivity for SABS glasses.

Composition	$[\Sigma Z_i(F_iV_i)/\Sigma Z_iV_i]_{\text{Network Former}}/[\Sigma F_iV_i/\Sigma V_i]_{\text{Network Former+Modifier}}$	$\Sigma O^+/\Sigma O^-+\Sigma O^+$	Glass network connectivity ψ (%)
SABS-0	1.40	0.53	74
SABS-5	1.38	0.52	72
SABS-10	1.37	0.48	66
SABS-15	1.36	0.49	66
SABS-35	1.31	0.37	48

second term represents the ratio of bridging oxygen atoms (O^+) versus the total oxygen atoms (O^- and O^+) in a glass network. ψ thus represents two aspects in a glass network: bonding effect of glass network cations and the ratio of bridging oxygen atoms versus the total oxygen atoms.

Based on the SABS glass compositions, the NMR spectra and the Raman spectra glass network connectivity for the SABS glasses has been calculated using Eq. (1) and the results are given in Table I. The field strength of SiO_2, Al_2O_3, La_2O_3, and SrO are 1.56, 0.97, 0.43, and 0.27, respectively, based on literature values and the cation function in the SABS glasses.[33] The field strength of B_2O_3 varies between 1.53 to 1.50 based on literature values and the BO_3:BO_4 ratios from SABS-0 to SABS-35.[33] As it shows, the bonding ability of glass network cations, the relative percent of bridging oxygen atoms, and the SABS glass network connectivity all decrease with B_2O_3 content increase. This result is very consistent with the NMR and Raman spectra, as well as the SABS glass thermal stability to be discussed. Glass connectivity serves as an important parameter in evaluating the thermal stability of a glass system.

While the connectivity calculation sheds new light on the glass network structure, it should be cautioned that the connectivity results in Table I involve two approximations. First, the amount of network forming cations contributed by Al^{3+} ions is unknown. Al_2O_3 participates in the glass network as a glass former but the relative amount decreases with B_2O_3 content increase. For the calculation in Table I, Al_2O_3 is assumed to always act as a glass former throughout the SABS glass composition range. Second, there are two Raman peaks for SABS-15 (1402 and 1438 cm^{-1}) and three Raman peaks for SABS-35 (1330, 1417, and 1443 cm^{-1}) that cannot be identified. In this calculation, they are assumed to come from borate structural units coordinated with glass modifiers. Detailed network structure analysis will be beneficial for addressing these two approximations and potentially provide more consistent trend.

Because of the configurational entropy difference between SiO_4 and BO_3 structural units, SiO_4 structural units preferentially link with BO_4 structural units, except for the linking among themselves. To understand the degree of bonding between SiO_4 and BO_4 units, two other related parameters can be calculated. One is the probability of silicon coordinated to BO_4 and the other is mean number of silicon coordinated to BO_4. SiO_4 and BO_4 structural unit coordination has been discussed previously but is desired to be further quantified. For a given glass, the mean number of silicon coordinated to BO_4 species is approximately constant and can be averaged over compositions of SABS-0 to SABS-35. Taking X_{Si} as the molar ratio of silicon to total network formers (silicon and boron) and assuming no BO_4 units are linked with each other, the mean number of silicon coordinated to BO_4 can be expressed as[34]

$$\langle l\rangle = \frac{16X_{\text{Si}}}{0.62 + 4.38X_{\text{Si}} - X_{\text{Si}}^2}. \tag{2}$$

The probability of silicon coordinated to BO_4 becomes

$$P(l) = \frac{4!}{l!\,(4-l)!}\left(\frac{4X_{Si}}{0.62 + 4.38X_{Si} - X_{\text{Si}}^2}\right)^l \times \left(\frac{0.62 + 0.38X_{Si} - X_{\text{Si}}^2}{0.62 + 4.38X_{Si} - X_{\text{Si}}^2}\right)^{4-l}. \tag{3}$$

Based on Eqs. (2) and (3), $\langle l\rangle$ and $P(l)$ can be calculated for the SABS glasses as shown in Fig. 5. $\langle l\rangle$ and $P(l)$ drastically decrease with B_2O_3 content increase. For SABS-5, the average mean number of silicon coordinated to BO_4 is 3.75; the probability $P(l)$ of finding silicon coordinated to BO_4 is 0.77. For SABS-35, the average mean number of silicon coordinated to BO_4 is 2.47; the probability $P(l)$ of finding silicon coordinated to BO_4 is 0.33. For SABS-10 and SABS-15, the values of $\langle l\rangle$ and $P(l)$ are in between the above ranges. This means as B_2O_3 content increases, there are not only fewer silicon atoms coordinated to BO_4 but the possibility of finding such coordination also drastically decreases. To put it differently, SiO_4 and BO_4 structural units are less and less likely to bond with each other with B_2O_3 content increase, even by assuming no BO_4 units are directly linked with themselves, an extreme assumption supported by the NMR results. This indicates that the glass network connectivity results in Table I should be considered jointly with the Q^n and T^n structural units distribution and bonding when evaluating a glass system, such as thermal stability.

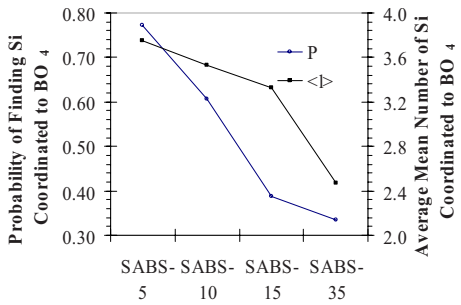

FIG. 5. (Color online) Probability of silicon coordinated to BO_4 and average mean number of silicon coordinated to BO_4 as a function of SABS glass composition.

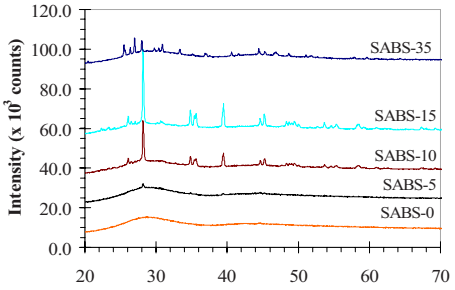

FIG. 6. (Color online) XRD patterns of SABS glasses thermally treated at 850 °C for 50 h.

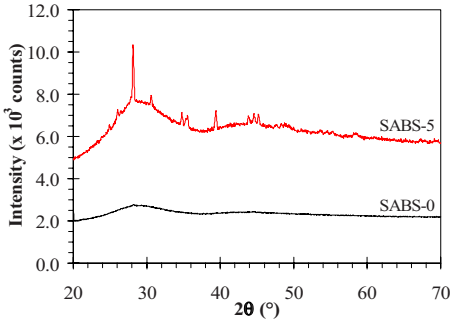

FIG. 7. (Color online) XRD patterns of SABS-0 and SABS-5 glasses thermally treated at 850 °C for 100 h.

D. Thermal stability

Glass network connectivity and homogeneity directly influence the devitrification resistance of a glass system. The decrease in glass network connectivity and the increase in glass structural unit inhomogeneity enhance the probability of glass devitrification. If structural unit local ordering occurs in a glass, even if only in small localized regions, the glass will be prone to devitrification, likely caused by heterogeneous nucleation.[7] For the studied SABS systems, the glass thermal stability can be evaluated by comparing the thermal treatment time to devitrification and the specific types of devitrified phases. Gibbs free energy change during the devitrification process may be the most precise approach to explain the devitrification tendency and the most likely devitrifying phase. However, thermodynamic data for the SABS glass systems at high temperatures are not available, especially for the species involving SrO and La_2O_3 modifiers. With the NMR and Raman spectra providing complementary data about BO_3:BO_4 ratios, environment of different structural units, as well as structural unit types, ordering, and distribution, XRD serves as an effective means to identifying the devitrified phases.

For the SABS glasses thermally treated at 850 °C for 50 h, the XRD patterns are given in Fig. 6. As can be seen, the SABS-0 glass shows no sign of devitrification after 50 h thermal treatment, suggesting that the SABS-0 glass is stable under such thermal treatment condition. The SABS-5 glass devitrifies after 50 h of thermal treatment. Small devitrification peaks are observed but the intensity and number of the peaks are insufficient to determine the devitrified phases. This result means SABS-5 is less stable than SABS-0 but not so unstable as to cause extensive devitrification. However, as B_2O_3 content continues to increase, SABS-10, SABS-15, and SABS-35 glass samples show more extensive devitrification after thermal treatment at 850 °C for 50 h. Monoclinic lanthanum silicate ($La_2Si_2O_7$) is the only phase in the SABS-10 glass. This means SiO_4 structural units interact with glass modifier La_2O_3. However, in the SABS-15 glass, three phases are identified. They are monoclinic lanthanum silicate ($La_2Si_2O_7$), rhombohedral aluminum borate ($AlBO_3$), and orthorhombic strontium boron aluminum oxide ($Sr_2B_2Al_2O_8$). In the SABS-35 glass, two phases, orthorhombic strontium borate (SrB_2O_4) and orthorhombic lanthanum borate ($LaBO_3$), are identified. $LaBO_3$ is the main phase. New phases in the SABS-15 and SABS-35 glasses can be seen in the new peak appearance and peak shifting in the XRD patterns from SABS-10 to SABS-15, then to SABS-35 (Fig. 6). Boron-containing devitrification phase appearance means that BO_3/BO_4 structural units become unstable and start to interact with glass modifiers (SrO and La_2O_3) and intermediate (Al_2O_3) along with SiO_4 structural units. The bonding energy of $Si-O-B^{III}$ bond is 119 kcal/mol, which is higher than that of $Si-O-B^{IV}$ bond at 89 kcal/mol.[35] Therefore, SABS glass thermal stability decreases as the amount of four-coordinated BO_4 units increases for higher B_2O_3 content. In addition, the SABS glasses contain La^{3+} and Sr^{2+} cations, which have a higher tendency to bond with the glass forming cations through nonbridging oxygen atoms than monovalent cations.[10,36] So, $La_2Si_2O_7$ is the major devitrified phases in all boron-containing SABS glasses except for SABS-35.

For the SABS-0 and SABS-5 glasses, which are more stable, Fig. 7 shows the XRD patterns after 100 h of thermal treatment at 850 °C. Still, the SABS-0 glass shows no signs of devitrification and continues to demonstrate itself as a very stable high temperature glass. For the SABS-5 glass, monoclinic $La_2Si_2O_7$ is the main phase along with small amounts of α-$SrSiO_3$ and Sr_2SiO_4 phases. This means when the glass network connectivity decreases, the T^n and Q^n structural units are less likely to bond with each other. SiO_4 structural units become more likely to interact with glass modifiers, such as SrO and La_2O_3, and form new species. This interaction leads to devitrification and Sr-containing crystalline phase formation. Nonetheless, the B_2O_3 content for the SABS-5 glass is low enough that the system is more stable than the other higher B_2O_3 content SABS glasses.

Figure 8 shows the XRD pattern of the SABS-0 glass after 200 h of thermal treatment at 850 °C. Very desirably, the SABS-0 glass is still amorphous with no devitrified

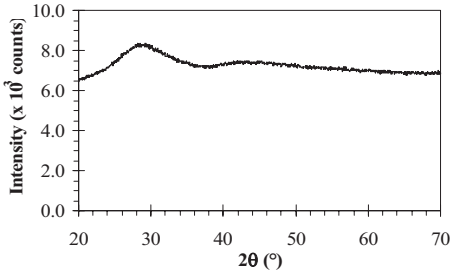

FIG. 8. XRD pattern of SABS-0 glass thermally treated at 850 °C for 200 h.

phase, demonstrated by the broad XRD pattern. This result is consistent with the glass network connectivity calculation. In Table I, the SABS-0 glass has the highest bonding ability, relative bridging oxygen content, and overall network connectivity. Therefore, the SABS-0 glass is the most thermally stable among all the studied glass compositions. This confirms that a glass network requires high connectivity for improved thermal stability. Absence of B_2O_3 content is conducive for bridging oxygen formation and devitrification resistance improvement.

With increasing B_2O_3 content, different devitrified phases evolve. This indicates that the devitrification process is accompanied by complex interaction among different glass structural units and glass modifiers. B_2O_3 decreases SABS glass network connectivity and glass structural unit coordination. The amount of bridging oxygen atoms decreases with the decrease in glass structure connectivity. The nonbridging oxygen atoms have a tendency to coordinate with the glass modifiers and form new species. The devitrified phase identification from the XRD study is consistent with the Raman data. In the SABS glasses, La^{3+} and Sr^{2+} ions act as modifiers. The intense peaks around 1028 cm^{-1} wave number in the SABS-10 and SABS-15 glasses suggest that the nonbridging oxygen atoms from the SiO_4 structural units may coordinate with La^{3+}.[37] Also, these La–O–Si containing linkages may be isolated and act as nucleation sites. Correspondingly, $La_2Si_2O_7$ phase is shown in the thermally treated SABS-10 and SABS-15 glasses from the XRD study. No Raman peak around 1028 cm^{-1} wave number is observed for SABS-5 even though $La_2Si_2O_7$ phase is present. This could be because the La–O–Si linkage content is too low to be detectable for SABS-5. For the SABS-35 glass, similar argument can be applied. Some nonbridging oxygen atoms are coordinated with Sr^{2+} ions and thus strontium-containing phases evolve. Several peaks above 1300 cm^{-1} wave number are similar to the crystalline phase $La(B_3O_6)$ peak in $BaO–La_2O_3–B_2O_3$ metaborate glass.[16] As a result, analogous structural units of $LaBO_3$ and Sr-metaborate are present, and $LaBO_3$ and SrB_2O_4 phases evolve.

With the understanding about the SABS glass network connectivity, glass structural unit coordination, and glass thermal stability, SABS glass network evolution process can be described as follows. At zero or low B_2O_3 content, SiO_4 glass network is highly connected; modifiers and a small amount of BO_3 structural units homogeneously distribute within the SABS glass. As B_2O_3 content increases, BO_4 structural unit content increases but the coordination with SiO_4 is rather weak; the BO_3 structural units change from metaborate to pentaborate. Substantial Q^n structural unit ordering and mixed bonding with the glass modifiers occur. Even though it is not possible to establish exact structure evolution model because of the complexity in bond formation between B–O–Si, Al–O–Si, B–O–Al, and modifiers, as well as gradual bond angle change, there is decreased coordination between SiO_4 and BO_4 structural units. Less connected BO_4 structural units interact preferably with the glass modifiers and new, unstable boron-containing crystalline species form.

IV. CONCLUSIONS

This study is focused on understanding the network connectivity, structural unit local ordering, and thermal stability of SABS glass system. Glass structural units and distribution were analyzed by NMR and Raman spectroscopy. Increasing B_2O_3 content causes glass network connectivity to decrease, glass structural unit local ordering, and glass former distribution inhomogeneity. This subsequently degrades SABS glass thermal stability, demonstrated by XRD results after thermal treatment at 850 °C for different periods of time. Depending on the bonding affinity with glass modifiers, silicon-containing devitrification phases form for low B_2O_3 content SABS glasses and boron-containing devitrification phases form for high B_2O_3 content SABS glasses. The most desired SABS glass is the B_2O_3-free composition, which remains stable after thermal treatment for 200 h at 850 °C.

ACKNOWLEDGMENTS

This material is based on work supported by the Department of Energy under Grant No. DE-FC07-06ID14739. The help of Mr. Charles Farley, Department of Geoscience, Virginia Tech during Raman spectroscopy experiment is highly appreciated. The authors also would like to acknowledge Professor Robert Bodnar, Department of Geoscience, Virginia Tech for his suggestions during Raman spectroscopy experiment, and Professor Sabyasachi Sen, Department of Chemical Engineering and Materials Science, University of California, Davis for the NMR experiment.

[1] EG & G Technical Services, *Fuel Cell Hand Book*, 7th ed. (US Department of Energy, Office of Fossil Energy, National Energy Technological Laboratory, Morgantown, West Virginia, 2004).
[2] K. L. Ley, M. Krumpelt, R. Kumar, J. H. Meiser, and I. Bloom, J. Mater. Res. **11**, 1489 (1996).
[3] M. K. Mahapatra, C. Story, K. Lu, and W. T. Reynolds, Jr., Proceedings of Materials Science and Technology 2007 Conference: Energy: Fuel Cells: Materials, Processing, Manufacturing and Power Management Technologies, edited by P. Singh, A.-M. Azad, D. C. Collins, P. N. Kumta, C. Legzdins, A. Manthiram, A. Manivannan, S. K. Sundaram, and Z. G. Yang, Detroit, Michigan, 16–20 September 2007 (unpublished), p. 371.
[4] M. K. Mahapatra, K. Lu, and W. T. Reynolds, Jr., J. Power Sources **179**, 106 (2008).
[5] M. J. Snyder, M. G. Mesko, and J. E. Shelby, J. Non-Cryst. Solids **352**, 669 (2006).
[6] S. T. Reis, R. K. Brow, T. Zhang, and P. Jasinski, Ceram. Eng. Sci. Proc. **27**, 297 (2006).
[7] W. Vogel, *Structure and Crystallization of Glass* (Pergamon, New York, 1971), p. 144.
[8] S. Sen, T. Topping, P. Yu, and R. E. Youngman, Phys. Rev. B **75**, 094203 (2007).
[9] S. Sen and P. Yu, Phys. Rev. B **72**, 132203 (2005).
[10] C. I. Merzbacher, B. L. Sherriff, J. S. Hartman, and W. B. White, J. Non-Cryst. Solids **124**, 194 (1990).
[11] L. S. Du and J. F. Stebbins, J. Non-Cryst. Solids **351**, 3508 (2005).
[12] B. N. Meera and J. Ramakrishna, J. Non-Cryst. Solids **159**, 1 (1993).
[13] P. McMillan, Am. Mineral. **69**, 622 (1984).
[14] R. K. Brow and D. R. Tallant, J. Non-Cryst. Solids **222**, 396 (1997).
[15] P. Boolchand, M. Jin, D. I. Novita, and S. Chakravarty, J. Raman Spectrosc. **38**, 660 (2007).
[16] S. A. Brawer and W. B. White, J. Non-Cryst. Solids **23**, 261 (1977).
[17] E. I. Kamitsos, J. A. Kapoutsis, H. Jain, and C. H. Hsieh, J. Non-Cryst. Solids **171**, 31 (1994).
[18] A. K. Hassan, L. M. Torell, L. Börjesson, and H. Doweidar, Phys. Rev. B **45**, 12797 (1992).
[19] B. O. Mysen, L. W. Finger, D. Virgo, and F. A. Seifert, Am. Mineral. **67**, 686 (1982).

[20]H. Li, P. Hrma, J. D. Vienna, M. Qian, Y. Su, and D. E. Smith, J. Non-Cryst. Solids **331**, 202 (2003).
[21]L. S. Du and J. F. Stebbins, J. Non-Cryst. Solids **315**, 239 (2003).
[22]W. J. Dell, P. J. Bray, and S. Z. Xiao, J. Non-Cryst. Solids **58**, 1 (1983).
[23]S. Kroeker and J. F. Stebbins, Inorg. Chem. **40**, 6239 (2001).
[24]R. Martens and W. Müller-Warmuth, J. Non-Cryst. Solids **265**, 167 (2000).
[25]B. C. Bunker, D. R. Tallant, R. J. Kirkpatrick, and G. L. Turner, Phys. Chem. Glasses **31**, 30 (1990).
[26]R. K. Brow, D. R. Tallant, and G. L. Turner, J. Am. Ceram. Soc. **79**, 2410 (1996).
[27]N. Ollier, T. Charpentier, B. Boizot, G. Wallez, and D. Ghaleb, J. Non-Cryst. Solids **341**, 26 (2004).
[28]F. L. Galeener, Phys. Rev. B **19**, 4292 (1979).
[29]F. Seifert, B. O. Mysen, and D. Virgo, Am. Mineral. **67**, 696 (1982).
[30]B. O. Mysen, D. Virgo, and F. A. Seifert, Am. Mineral. **70**, 88 (1985).
[31]J. E. Shelby, *Introduction to Glass Science and Technology* (Royal Society of Chemistry, Cambridge, 2005).
[32]M. B. Volf, *Chemical Approaches to Glass: Glass Science and Technology* (Elsevier, Amsterdam, 1984), Vol. 7, p. 100.
[33]H. Scholze, *Glass Nature, Structure and Properties* (Springer-Verlag, New York, 1991), p. 109.
[34]L. S. Du and J. F. Stebbins, J. Phys. Chem. B **107**, 10063 (2003).
[35]W. F. Du, K. Kuraoka, T. Akai, and T. Yazawa, J. Phys. Chem. B **105**, 11949 (2001).
[36]S. K. Lee, B. O. Mysen, and G. D. Cody, Phys. Rev. B **68**, 214206 (2003).
[37]A. J. G. Ellison and P. C. Hess, J. Non-Cryst. Solids **127**, 247 (1991).